Application of mathematical search algorithms for unknown material properties in Additive Manufacturing simulations

Aaron Flood[1] and Frank Liou[1]

[1]Mechanical and Aerospace Engineering, 194 Toomey Hall, Rolla, 65409, MO, USA.

Contributing authors: ajfrk6@umsystem.edu; liou@umsystem.edu;

Abstract

Additive manufacturing (AM) simulations have risen as a way to better understand the effect of processing parameters on builds. They are effective for materials which are well characterized and published, however for newer or proprietary materials, they cannot provide accurate results due to the lack of knowledge of material properties. This work demonstrates the process of the application of mathematical search algorithms to develop an optimized material dataset which result in accurate simulations. This was done with 7000 series aluminum and the laser directed energy deposition (DED) process. The Nelder-Mead search algorithm was able to develop an optimized dataset which had a combined width and depth error of just 9.1% when starting from generic aluminum material properties found in literature which had an initial error of 600%.

1 Introduction

1.1 Additive manufacturing (AM) simulations

Additive manufacturing (AM) is an emerging manufacturing technique which has the potential to revolutionize manufacturing. In order to realize this revolution, it is necessary to be able to produce components reliably and to understand the process well enough to ensure that builds are consistent enough that the performance of the completed build can be guaranteed. In order to

do this, researchers and manufacturers have turned to mathematical modeling to understand the process Wang and Chen (2021).

The differences in simulation techniques can vary based on the desired response from the simulation and the underlying assumptions which were made during the development of the models. One example of this can be seen when comparing the mathematical models presented in Wang and Chen (2021), Roy and Wodo (2020), and Moges et al (2020). They all attempt to model roughly the same aspect of the build but take very different approaches. Wang and Chen (2021) take a purely physics-based approach to the solution and works from first principal of the physical process being modeled. On the contrary, Roy and Wodo (2020) is a data driven model which used a breadth of data to develop a mathematical model which properly predicts the material behavior. In between these models exists Moges et al (2020) which attempts to marry the two approaches and develop a physics-based model which uses data to improve accuracy. The one unifying characteristic of these, and all, mathematical models, is the need for the inclusion of a dataset which defines the behavior of material being investigated, this is colloquially referred to as the material properties. These material properties can vary in literature and this variance in values can lead to a discrepancy in simulation results Daryabeigi (2011).

Though variation exists in the literature, values can be found and used when the material is well characterized and published. An example of a well published material is Ti-64 where it is easy to find literature which reports the material properties such as in Welsch et al (1993), Boivineau et al (2006), and Fan and Liou (2012). However, for materials which are not well understood and published, such as specific aluminum alloys it can be very challenging though possible with Lundberg (1994) and Leitner et al (2017), there is a need to determine the material properties, or at a minimum, develop the dataset which produces the most accurate simulation results. This can be accomplished by expending the necessary resources to measure the needed properties using advanced equipment. This process can be expensive and time-consuming which has led to the development of material simulations which attempt to predict the material properties. Though faster and cheaper than experimental results, they, like all simulations, have an error that is associated with them. Using these values alone can lead to unknown error stack up in the AM models. This problem also applies to materials where the tolerances for alloying elements is so wide that specimen of the same alloy can have different material properties.

In order to develop a dataset which produces accurate AM simulation results, a multi-objective optimization scheme can be used as a search algorithm to determine the dataset which produces the most realistic results. This can be used to develop a dataset for a new alloy along with for a specific batch of stock which has been procured from a supplier.

This work will aim to address one of the current desires in metal AM which is to be able to produce parts out of aluminum. This desire is evident by the volume of effort being put into aluminum AM (Qi (2020), Weiss (2019b), Weiss (2019a)). The challenge associated with this stems from the wide range

of alloys which have wildly varying material properties which are not well published. One of the weldable high strength alloys which has been targeted for metal AM is 7050 Singh (2017). Though the material is widely available, temperature dependent material properties are not readily available. Therefore, this work will find material properties in literature which are an approximation of the 7050 aluminum, namely sister alloys with similar compositions, as a starting point for the search algorithm and determine a material dataset which produces more accurate AM simulation results.

1.2 Simulation description

The model used in this study was developed at Missouri University of Science and Technology and is detailed in **??**. This simulation has the express goals of being efficient while still holding true to physics models. In order to accomplish this, it heavily leverages GPU processing utilizing image processing techniques. The simulation was developed with laser DED processes in mind, however, it was developed in a modular manner such that it can be applied to most AM processes.

The main objective of the model is to accurately predict the thermal history of the build. This was shown to be true in **??** where the model was able to predict the width of the melted track with approximately 3% error and the depth within 1.7 resolution steps (which was approximately 20% error) for the well published material of Ti-64.

2 Tuning algorithm implementation

2.1 Tuning algorithm description

The search algorithm which was chosen was the Nelder-Mead search algorithm Nelder and Mead (1965). This method was selected because it is one of the most popular direct search methods for minimization of functions. The Nelder-Mead approach is a local optimization search which does not rely on knowledge of the gradient to select the next search point. This is critical for the application to simulation results because the gradient is unknown and finding it would involve running a large number of simulations. With simulation times that can reach into days long, this is a critical consideration. Instead of knowing the actual function, it relies on n+1 vertices. This means that a smaller number of simulation runs are needed to perform the minimization Wang and Shoup (2011). The flow chart in Figure 1 is the flow which is used to determine the next search point.

In general, for each time step the reflection point is calculated using Equation 1 where α is the reflection coefficient.

$$P_{refl} = (1 + \alpha)P_{cent} - \alpha P_{high} \tag{1}$$

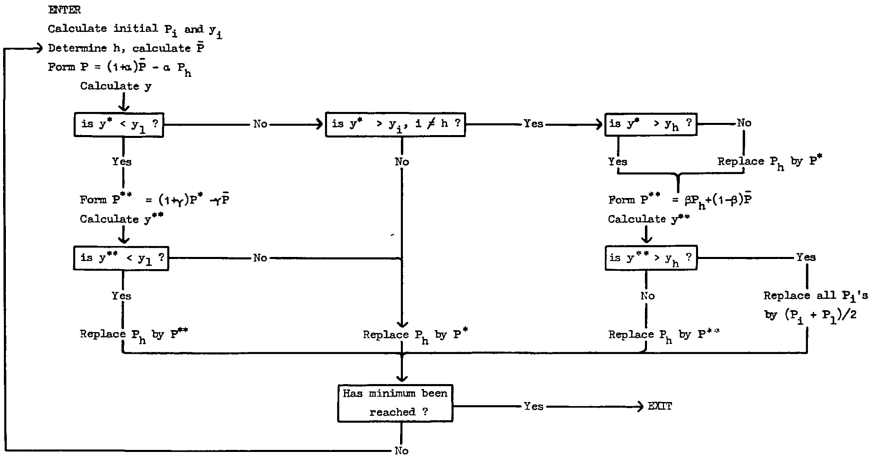

Fig. 1: Flow chart for the Nelder-Mead search algorithmNelder and Mead (1965)

If this reflection point is smaller than the smallest current simplex value, then the expansion is calculated using Equation 2, where γ is the expansion coefficient.

$$P_{exp} = \gamma P_{refl} - (1 - \gamma)P_{center} \tag{2}$$

If the expansion point is smaller than the reflection point then the expansion point is used to replace the largest simplex member. Otherwise, if the reflection point is larger than the expansion point the reflection point is used to replace the largest member of the simplex, and the algorithm is restarted. If the reflection point is larger than the smallest simplex point and smaller than the second largest point then the highest point of the simplex is replaced with the reflection and the algorithm is restarted. If the reflection point is between the simplex high and second highest value, a contraction is calculated, using Equation 1 with the highest values being replaced with the reflection, otherwise the contraction is calculated with the original simplex still using Equation 1, where β is the contraction coefficient.

$$P_{cont} = \beta P_{high} - (1 - \beta)P_{cent} \tag{3}$$

If the contraction point is smaller than the largest point of the simplex the contraction replaces the largest point and the algorithm is continued. However if the contraction point is larger than the highest point, a shrink step is performed, detailed in Equation 4, where δ is the shrink coefficient, and the algorithm is restarted.

$$P_i = \delta P_i + (1 - \delta)P_{low} \tag{4}$$

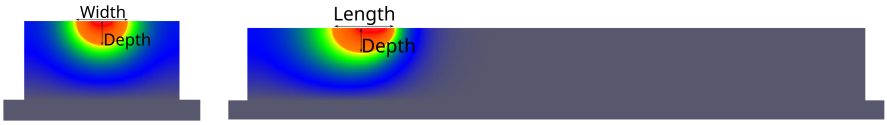

(a) Width (b) Length

Fig. 2: Example measurements of the melt pool

2.2 Selection of Properties

One of the attractive characteristics of the Nelder-Mead search algorithm, is its ability to sale to an unlimited number of unknowns. The main adverse effects are the increased number of runs and the combination of the errors. As the number of unknown increases the complexity of the search space increases, which in turn increases the number of iterations needed to find a minimum. This can result in drastically longer wait times on search results. Additionally, with the increased number of unknowns, the stop condition of the search algorithm will be met at a different interval since the stop condition is based on the variance in the simplex. This may result in modifications to the stop conditions being necessary as larger number of unknowns are included. If the response variable is properly defined, it will not affect the models results if more unknowns are included Wang and Shoup (2011).

In order to reduce the complexity of the search algorithm, a sensitivity analysis was performed in **??**. This work began by finding the material properties which were needed in the models as summarized in Table 1.

Table 1: Key material properties in thermal modeling of AM

Material Property	Reference
Solidus temperature	Joseph R. Davis (2001), Lundberg (1994), Ulbirch (2014), ASM (2022)
Liquidus temperature	Joseph R. Davis (2001), Lundberg (1994), Ulbirch (2014), ASM (2022)
Solid density	ASM (2022), AmesWeb (2022)
Fluid density	ASM (2022), Schmitz et al (2012), Leitner et al (2017)
Specific heat	Lundberg (1994), Leitner et al (2017)
Thermal conductivity	Lundberg (1994), Leitner et al (2017)
Absorptivity	Funck et al (2014), Boyden and Zhang (2006), El-Hameed et al (2017)

These properties were varied according to a Placket-Burman design of experiment in order to determine the properties which, when changed, had a statically significant effect on the resulting melt pool width, depth, and volume, as measured in Figure 2. Analyzing these results with Pareto charts of the standardized effects of the variables and partial regression plots of the residuals it was determined that the variables in Table 2 had a statically significant

effect on the resulting melt track when modified. This work included the laser

Table 2: Critical material properties

Laser absorption at 880°C
Laser absorption at 922°C
Thermal conductivity at 922°C
Thermal conductivity at 1491°C
Specific heat at 733°C

diameter in the search algorithms dataset due to the difficulty associated with accurately measuring the diameter.

2.3 Tuning and Simulation setup

For this study, the Nelder Mead search algorithm parameters which were used can be seen in Table 3. These parameters were chosen because they fell within

Table 3: Nelder-Mead algorithm parameters

Parameter	Value
α	5.0
γ	10.0
β	0.5
σ	0.5

the guidelines from the algorithm description and after trial and error produced the most efficient tuning Nelder and Mead (1965).

The starting values which were used as the starting point for the search algorithm can be seen in Table 4. These values were chosen based on the values which were found in literature for similar aluminum alloys. The laser diameter which was chosen based on the measuring of a melt track width on a substrate.

Table 4: Material properties found in literature

Property	Material Temp.	Value	Ref.
Laser absorption	880°C	15.0%	Boyden and Zhang (2006)
Laser absorption	922°C	30.0%	Boyden and Zhang (2006)
Thermal conductivity	922°C	88.8 $\frac{W}{mK}$	Leitner et al (2017)
Thermal conductivity	1491°C	104.9 $\frac{W}{mK}$	Leitner et al (2017)
Specific heat	733°C	1108.0 $\frac{J}{kgK}$	Leitner et al (2017)
Laser diameter		1.6 mm	

The experimental setup which was used as a simple laser scanning of the surface of a substrate, as shown in Figure 3, with the parameters shown in Table 5. This was chosen in order to simplify the experiment. This setup removes the complexity associated with adding material including the rate

of material addition, molten metal flow parameters, and acceleration effect associated with turning during deposits.

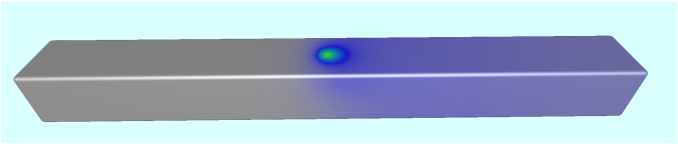

Fig. 3: Example of simulation setup used to determine melt track size

Table 5: Experimental constants used in tuning experiments

Parameter	Value
Resolution	100 μm
Laser Power	1,750 W
Laser Scan Speed	1143 mm/min
Laser Profile	Top Hat
Scan Length	77 mm
Substrate dimensions	82 mm x 8 mm x 8 mm

2.4 Simulation analysis

Upon completion of each simulation run, the saved data files were analyzed to determine the regions of the simulation which had melted. This was done by developing a map which marked the locations of the domain which had ever been in the fluid phase. This map was then used to determine the width and depth of the melt track along the scan length, excluding the beginning and end where effects from starting and stopping motion would affect the results. These width and depth measurements along the scan length were averaged to develop a single measurement which could be compared to experimentation.

The experimental results were similarly determined, however instead of a continuous set of measurements, there were 4 discrete measurements. These were obtained by slicing the substrate at the prescribed locations using a Wire electrical discharge machine (EDM). These slices were polished and etched in order to make the microstructural differences visible, an example of this can be seen in Figure 4, where the dark region had been melted during the experimentation.

In order for the Nelder-Mead search to function properly, a response variable needed to be defined. This function needed to characterize the accuracy of the simulation into a single parameter which could be minimized and upon minimization would result in the most accurate simulation. To accomplish this goal, Equation 5 was developed. This equation takes into account the error in the width of the simulation along with the error of the depth. This

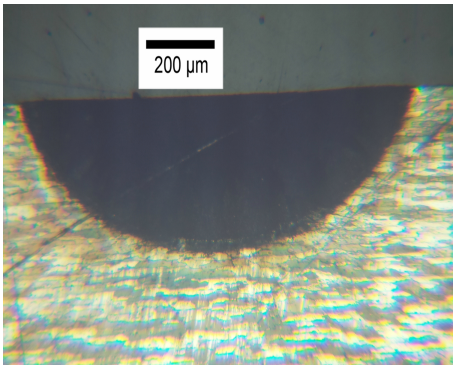

Fig. 4: Example of sliced, polished, and etched slice from experimentation

equation results in a non-negative number where 0 represents a simulation which perfectly matched experimentation.

$$Response = \left(\frac{|Sim.\ Width - Exp.\ Width|}{Exp.\ Width} + \frac{|Sim.\ Depth - Exp.\ Depth|}{Exp.\ Depth} \right) * 100 \tag{5}$$

3 Results

3.1 Search algorithm results

The search algorithm was allowed to search the space to determine the best material properties. The resulting response variables can be found in Figure 5. Where the blue circular markers indicate material datasets which developed a melt track and the red diamond markers did not have the energy density to produce a melt track. Due to the vast difference in scales of the initial responses and the final response variables, a new plot was created which has a max Y value of just over 30. In this plot the blue circular markers are ones which have a response variable less than 30, the green triangle markers are those which completed with a melt track but had response variables greater than 30, and the red diamond markers are those which did not produce a melt track. In addition to these plots the error in the width and depth were plotted and can be seen in Figure 7. In these plots, it can be seen that the error in the width is 8.83% and the error in the depth is 0.03%. It is not fully understood why all the error is coming from width, however it is theorized that this is a product of difference in the size of the width vs the depth since the width is nearly triple that of the depth.

The search algorithm completed and reduced the combined error from over 600% when starting from the material properties found in literature for the

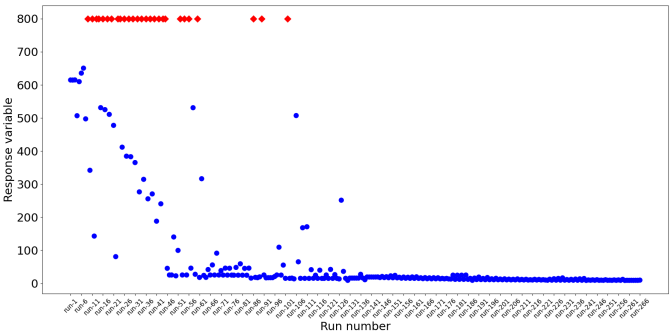

Fig. 5: Response variable of the search algorithm for material properties and laser diameter

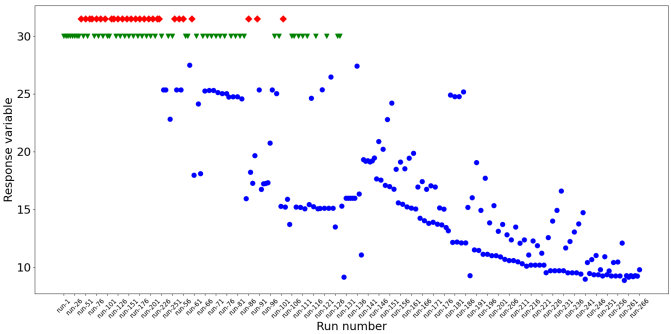

Fig. 6: Response variable of the search algorithm for material properties and laser diameter with max y axis value of 30

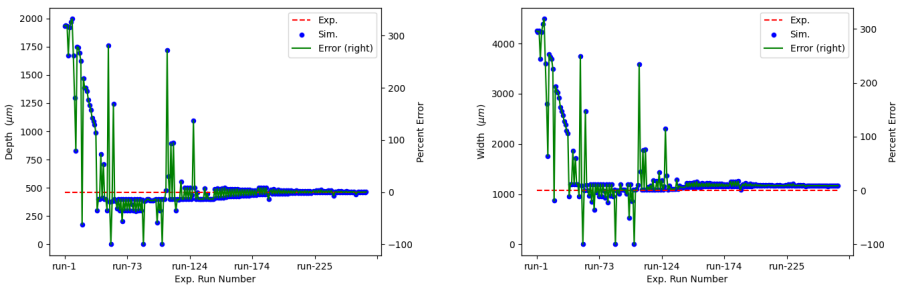

(a) Melt track depth (b) Melt track width

Fig. 7: Error in the individual runs of the simulations during the tuning algorithm

generic aluminum material properties, found in Table 4, to 9.1% when using the values found in Table 6

Table 6: Optimized material properties and laser diameter dataset for the developed simulation

Property	Material Temp.	Value
Laser absorption	880°C	16.8%
Laser absorption	922°C	10.0%
Thermal conductivity	922°C	32.2 $\frac{W}{mK}$
Thermal conductivity	1491°C	152.3 $\frac{W}{mK}$
Specific heat	733°C	2957.6 $\frac{J}{kgK}$
Laser diameter		0.864 mm

3.2 Search results validation

In order to ensure that the search algorithm results were valid across laser travel speeds and power levels a range of 8 other parameters were compared, the values used can be seen in Table 7.

Table 7: Validation processing parameters

Exp. Id.	Scan speed (mm/min)	Laser Power (W)
1	762	1000
2	762	1500
3	762	1250
4	1143	1250
5	1143	1500
6	1524	1750
7	1524	1500
8	1524	2000

These speeds and powers were first completed with the literature determined values from Table 4 and the results can be seen in Figure 8. These results show that over the 9 initial parameter sets, when a melt track was developed, the average absolute value of the error in the depth was approximately 290% and the average error in the width was approximately 265%. And to put into terms of the response variable of the search algorithm, the sum of the width and depth error, would be 555% combined error. Additionally, run 1 was unable to develop a melt pool, which is contrary to the experiments where all the parameter sets had a stable melt track. These results corroborate the results from Figure 5 which showed that for the parameter set used for tuning initial dataset of material properties found in literature is wholly inadequate for simulating the process at hand.

In contrast to these results, the material dataset which was found in Table 6 was used to simulate each parameter set, and the results can be seen in

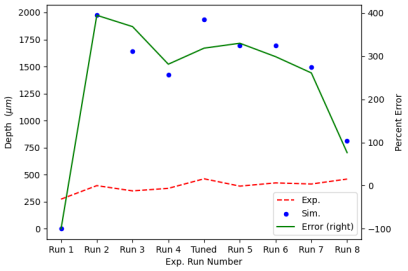

(a) Melt track depth

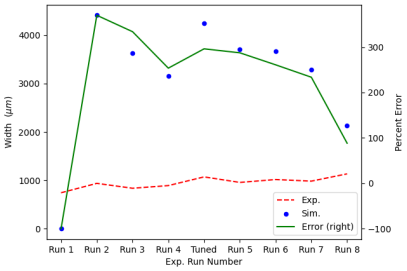

(b) Melt track width

Fig. 8: Comparison of experimental and simulated results for validation points

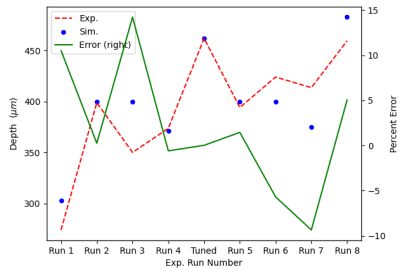

(a) Melt track depth

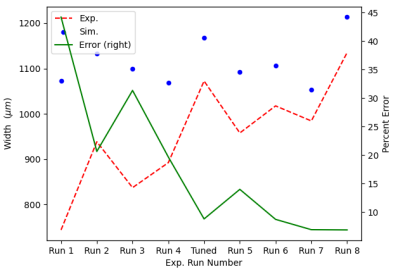

(b) Melt track width

Fig. 9: Comparison of experimental and simulated results for validation points

Figure 9. These results show the average error in the width was approximately 17% and the average error in the depth was approximately 5%, which create a combined error of only 22%. These results show that the optimized dataset is better at predicting the combined error of the simulation by over 500%. This results in a simulation which can be leveraged more intensely during the process development and build qualification process.

4 Conclusions

This work shows that the Nelder-Mead search algorithm is an appropriate multidimensional search algorithm for the determination of the optimal dataset for improved simulation accuracy. It was capable of reducing the simulated melt track depth and width of a set of processing parameters by over 500%, as shown in Figures 8 and Figure 9, which used datasets from literature (Table 4) and the optimized dataset (Table 6) respectively. This was done by defining the response variable (Equation 5) for the search algorithm to be the sum of the error in the width and the depth, which facilitated an efficient search. This

methodology can be used to develop accurate simulations for any material which is not well published or to increase the accuracy of a simulation which utilizes approximations of first principals in order to increase its efficiency.

References

AmesWeb (2022) ALUMINUM 6061 MATERIAL PROPERTIES. https://amesweb.info/Materials/Aluminum-6061-Properties.aspx

ASM (2022) Aluminum 6061-T6; 6061-T651. http://asm.matweb.com/search/SpecificMaterial.asp?bassnum=MA6061T6

Boivineau M, Cagran C, Doytier D, et al (2006) Thermophysical Properties of Solid and Liquid Ti-6Al-4V (TA6V) Alloy. International Journal of Thermophysics 27(2):507–529. https://doi.org/10.1007/PL00021868

Boyden SB, Zhang Y (2006) Temperature and Wavelength-Dependent Spectral Absorptivities of Metallic Materials in the Infrared. Journal of Thermophysics and Heat Transfer 20(1):9–15. https://doi.org/10.2514/1.15518

Daryabeigi K (2011) Thermal Properties for Accurate Thermal Modeling

El-Hameed AMA, Abdel-Aziz YA, El-Tokhy FS (2017) Anodic Coating Characteristics of Different Aluminum Alloys for Spacecraft Materials Applications. Materials Sciences and Applications 08(02):197–208. https://doi.org/10.4236/msa.2017.82013

Fan Z, Liou F (2012) Numerical Modeling of the Additive Manufacturing (AM) Processes of Titanium Alloy. In: Amin AN (ed) Titanium Alloys - Towards Achieving Enhanced Properties for Diversified Applications. InTech, https://doi.org/10.5772/34848

Funck K, Nett R, Ostendorf A (2014) Tailored Beam Shaping for Laser Spot Joining of Highly Conductive Thin Foils. Physics Procedia 56:750–758. https://doi.org/10.1016/j.phpro.2014.08.082

Joseph R. Davis (2001) Aluminum and Aluminum Alloys Davis.pdf. In: Alloying: Understanding the Basics. ASM International

Leitner M, Leitner T, Schmon A, et al (2017) Thermophysical Properties of Liquid Aluminum. Metallurgical and Materials Transactions A 48(6):3036–3045. https://doi.org/10.1007/s11661-017-4053-6

Lundberg S (1994) Material Aspects of Fire Design

Moges T, Yang Z, Jones K, et al (2020) HYBRID MODELING APPROACH FOR MELT POOL PREDICTION IN LASER POWDER BED FUSION

ADDITIVE MANUFACTURING p 15

Nelder JA, Mead R (1965) A Simplex Method for Function Minimization. The Computer Journal 7(4):308–313. https://doi.org/10.1093/comjnl/7.4.308

Qi Y (2020) A high strength Al–Li alloy produced by laser powder bed fusion_ Densification, microstructure, and mechanical properties. Additive Manufacturing p 10

Roy M, Wodo O (2020) Data-driven modeling of thermal history in additive manufacturing. Additive Manufacturing 32:101,017. https://doi.org/10.1016/j.addma.2019.101017

Schmitz J, Hallstedt B, Brillo J, et al (2012) Density and thermal expansion of liquid Al–Si alloys. Journal of Materials Science 47(8):3706–3712. https://doi.org/10.1007/s10853-011-6219-8

Singh A (2017) Additive Manufacturing Of Al 4047 And Al 7050 Alloys Using Direct Laser Metal Deposition Process. PhD thesis

Ulbirch (2014) 6000 & 7000 Series Aluminum Alloy

Wang D, Chen X (2021) Closed-Loop High-Fidelity Simulation Integrating Finite Element Modeling With Feedback Controls in Additive Manufacturing. Journal of Dynamic Systems, Measurement, and Control 143(2):021,006. https://doi.org/10.1115/1.4048364

Wang PC, Shoup TE (2011) Parameter sensitivity study of the Nelder–Mead Simplex Method. Advances in Engineering Software 42(7):529–533. https://doi.org/10.1016/j.advengsoft.2011.04.004

Weiss D (2019a) Developments in Aluminum-Scandium-Ceramic and Aluminum-Scandium-Cerium Alloys. In: Chesonis C (ed) Light Metals 2019. Springer International Publishing, Cham, p 1439–1443, https://doi.org/10.1007/978-3-030-05864-7_180

Weiss D (2019b) Improved High-Temperature Aluminum Alloys Containing Cerium. Journal of Materials Engineering and Performance 28(4):1903–1908. https://doi.org/10.1007/s11665-019-3884-2

Welsch G, Boyer R, Collings E (1993) Materials Properties Handbook: Titanium Alloys. ASM international